ACCSCIENCE PUBLISHING

International Journal of Bioprinting

RESEARCH ARTICLE

Bioprinting vascularized human islet tissue models via aggregate-based co-culture and self-assembly

Yijun Su[1,2†], Supeng Ding[2,3†], Tiankun Liu[2], Yongyong Zhou[2], Yinying Lu[1,2], Feng Lin[1], Mingen Xu[4*], and Rui Yao[1,2,5*]

[1]Biomanufacturing and Rapid Forming Technology Key Laboratory of Beijing, Department of Mechanical Engineering, School of Mechanical Engineering, Tsinghua University, Beijing, China

[2]Human Organ Physiopathology Emulation System, Institute of Zoology, Chinese Academy of Sciences, Beijing, China

[3]Department of Materials Science and Engineering, Institute for Nanobiotechnology, Johns Hopkins University, Baltimore, MD, United States

[4]Key Laboratory of Medical Information and 3D Bioprinting of Zhejiang, School of Automation, Hangzhou Dianzi University, Hangzhou, Zhejiang, China

[5]Beijing Institute for Stem Cell and Regenerative Medicine, Beijing, China

(This article belongs to the *Special Issue: 3D Bioprinting and Stem Cells for Human Tissue Reconstruction*)

Abstract

Diabetes is a significant global metabolic disease. Current treatments, including islet or pancreas transplantation and insulin therapy, are limited by donor shortages and suboptimal glycemic control. Islet organoids, three-dimensional (3D) cell aggregates that mimic pancreatic islets, offer a powerful tool for diabetes research, drug screening, and transplantation therapies. However, challenges remain in engineering methods for the scalable preparation of human islet organoids (hIOs) with homogeneous consistency and controllable incorporation of vascular elements. In this study, we developed a novel bioengineering approach for the stable production of human islet tissue models with vascular elements using a combination of 3D bioprinting-based organoid co-culture and cell self-assembly principles. Human adipose-derived mesenchymal stem cells were differentiated into massive and uniform human islet β-like cell aggregates (hICAs) using an off-the-shelf polydimethylsiloxane user-defined micropatterning platform system. A tri-module thermal-controlled bioprinting process employing a gelatin–alginate–Matrigel bioink was used for the 3D bioprinting of hICAs and human umbilical vein endothelial cells (HUVECs). Compared with bioprinted hICAs alone, co-bioprinted and co-cultured hICAs and HUVECs more effectively recapitulated the morphogenesis of human islet development, significantly upregulated the expression of pancreatic islet- and endothelial cell-related markers, and enhanced islet function, namely glucose-stimulated insulin secretion. Thus, the self-assembly of hICAs and HUVECs to form hIOs with vascular elements mimics natural human pancreatic islets and may promote functional maturity. Our method provides a scalable platform for generating vascularized aggregation-based tissue models, supporting studies of pancreatic development and diabetes therapy.

Keywords: Bioprinting; Human adipose-derived mesenchymal stem cells; Human islet tissue models; Islet β-like cell aggregates

†These authors contributed equally to this work.

***Corresponding authors:**
Rui Yao (yaorui@ioz.ac.cn)

Mingen Xu (xumingen@hdu.edu.cn)

Citation: Su Y, Ding S, Liu T, *et al.* Bioprinting vascularized human islet tissue models via aggregate-based co-culture and self-assembly. *Int J Bioprint*. 2025;11(6):279-297. doi: 10.36922/IJB025360368

Received: September 6, 2025
Revised: October 1, 2025
Accepted: October 2, 2025
Published online: October 7, 2025

1. Introduction

Diabetes is a global health crisis that affects approximately 540 million adults worldwide, posing significant socioeconomic challenges.[1] Current treatments, such as insulin (INS) therapy and islet or pancreas transplantation, offer varying degrees of success but have limitations, including a shortage of donor tissues, the risk of immune rejection, and suboptimal glycemic control.[2] Recently, human islet organoids (hIOs) have emerged as an alternative to address these challenges. Islet organoids are three-dimensional (3D) cell aggregates that closely resemble pancreatic islets, consisting of INS-producing β-cells and stromal cell types.[3] Their advantages include the capacity to model islet development and function *in vitro*, as well as reduced dependence on donor islets for transplantation, making them highly promising for diabetes research, drug screening, and transplantation therapies.[3,4]

Generating hIOs from embryonic stem cells (ESCs) and induced pluripotent stem cells (iPSCs) has shown great promise in mimicking pancreatic islet functions. However, several limitations hinder their large-scale application.[5,6] ESCs raise ethical concerns since they are derived from human embryos, which creates regulatory challenges. Additionally, both ESCs and iPSCs require complex differentiation protocols, which are prone to variability, leading to inconsistent phenotypes and functions, as well as the risk of tumorigenicity due to residual undifferentiated cells. Moreover, the production scale is limited due to the costly, labor-intensive, and time-consuming nature of these differentiation processes, making it challenging to meet research and clinical demands.[7] In contrast, human adipose-derived mesenchymal stem cells (hADSCs) offer a compelling alternative. hADSCs are mesenchymal stem cells derived from adipose tissue. They are abundant, exhibit low immunogenicity, and possess the potential for mesenchymal lineage differentiation, with significant implications for regenerative medicine.[8] Previous studies have shown that hADSCs can differentiate into INS-producing β-like cells under planar culture conditions, positioning them as a viable candidate for producing functional hIOs on a larger scale.[9,10]

The production of human islet tissue models is constrained not only by the cell source but also by the need to create a complex microenvironment that allows adequate mass transfer. Bioprinting has emerged as a promising technique for creating 3D microenvironments in which extracellular matrix-mimicking hydrogels and cellular components, such as cells, cell aggregates, and organoids, can be spatially positioned.[11,12] Previous studies have demonstrated that 3D bioprinting effectively supports cell-aggregate integrity, spatial organization, and the functional maturation of islets derived from various cell sources, including primary human islets[13] and ESC-derived[14] and iPSC-derived[15] islet-like cell aggregates. While these studies enhanced matrix complexity through bioprinting, they typically focused on a single cell type, namely β-cells, and thus lacked the multicellular characteristics of actual islet tissues. This is particularly important because islet tissues are highly vascularized. Recent research has highlighted the importance of endothelial-derived signals in enhancing the viability and function of insulin-producing cells in bioprinted co-culture models.[16,17] However, due to the technical challenges associated with bioprinting multiple cell types and cell aggregates, current co-bioprinting methods are still limited to single-cell-based formats and have not yet succeeded in the scalable preparation of functional human islet tissue models that incorporate vascular elements in a controlled manner.

In this study, we propose a systematic solution that involves the stepwise preparation of large-scale, uniform cell aggregates and the precise regulation of cell-printing technology to create human islet tissue models featuring multicellular crosstalk and islet functionality similar to that of natural islets. To enable large-scale generation of uniform cell aggregates, we developed an off-the-shelf polydimethylsiloxane (PDMS) user-defined micropatterning platform (PUMP). This system incorporates micro-engineered microwells shaped like inverted pyramids, which possess favorable mechanical properties. Upon differentiation of hADSCs, the PUMP system successfully generated large numbers of human islet β-like cell aggregates (hICAs). The hICAs formed in the PUMP system displayed a more uniform size distribution, enhanced expression of pancreatic islet marker genes, and reduced expression of stemness marker genes compared to those generated by planar culture and the AggreWell plate, a commonly used commercial cell-aggregation platform.

To incorporate vascular elements, we propose a tri-module thermally controlled bioprinting method utilizing an optimized ternary gelatin–alginate–Matrigel bioink. This method enables the bioprinting of hICAs alongside human umbilical vein endothelial cells (HUVECs) into co-culture tissue models. After 5 days of culture following bioprinting, HUVECs migrated and enveloped the surface of the hICAs, forming an endothelial layer and resulting in hIOs that included vascular elements, indicating self-assembly and multicellular crosstalk. In comparison to the bioprinted hICAs alone, the co-cultured hIOs exhibited significantly increased expression of islet-marker genes and enhanced islet functionality, including adequate glucose-stimulated INS secretion (GSIS) (Figure 1). This study presents a novel approach for generating large-scale

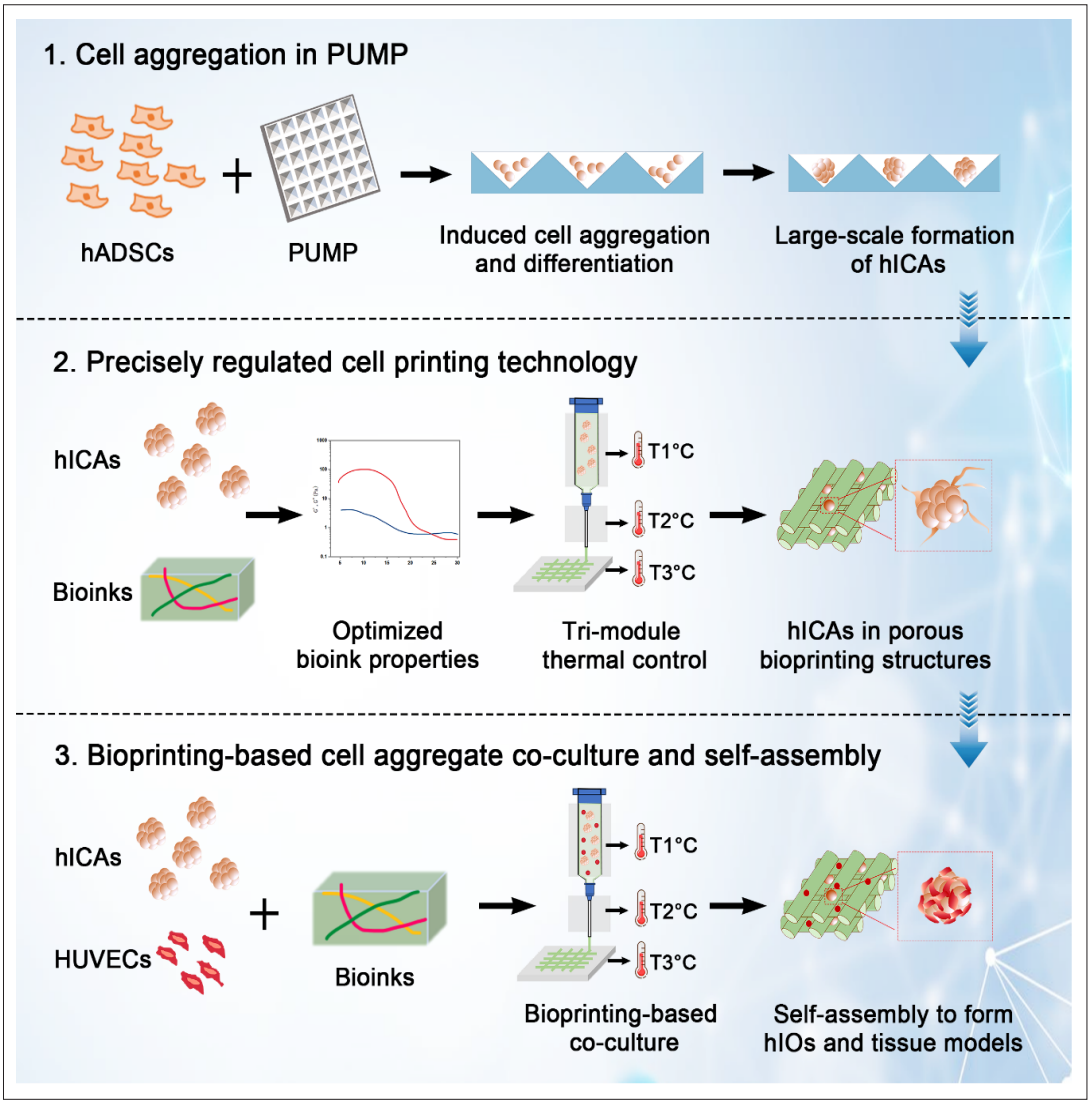

Figure 1. Schematic diagram of the study. Abbreviations: hADSC, human adipose-derived stem cell; hICA, human islet β-like cell aggregate; hIO, human islet organoid; HUVEC, human umbilical vein endothelial cells; PUMP, polydimethylsiloxane user-defined micropatterning platform.

human islet models that facilitate vascular integration and enhanced tissue function, thereby advancing diabetes research and paving the way for engineered therapeutic islet transplants.

2. Materials and methods

2.1. Solution preparation

Human adipose-derived stem cell–islet β-cell differentiation medium, sodium alginate working solution, and gelatin working solution were prepared as follows:

(i) hADSC–islet β-cell differentiation medium: The medium was optimized based on the protocol by Dave *et al.*[10] Briefly, the differentiation medium consisted of Dulbecco's Modified Eagle Medium (DMEM; Gibco, USA) and DMEM/F-12 medium (Gibco, USA) mixed at 1:1 (v/v) ratio, supplemented with 2% B-27 supplement (Gibco, USA), 1% N-2 supplement (Gibco, USA), 10 mM nicotinamide (Sigma-Aldrich, USA), 2 nM human activin A (R&D Systems, USA), 10 nM exendin-4 (Sigma-Aldrich, USA), 10 nM pentagastrin (Sigma-Aldrich, USA), 100 pM human hepatocyte growth factor (R&D Systems, USA), and 1% penicillin–streptomycin (Solarbio, China).

Sodium alginate working solution (4% [w/v]): Sodium alginate powder (Sigma-Aldrich, USA) was dissolved in the 0.9% sodium chloride (NaCl; Sigma-

Aldrich, USA) solution. The solution was heated at 80°C for 3 h, followed by stirring at 750 rpm for 1 h at 37°C on a magnetic stirrer (MS-H340-S4, DLAB, China). The heating and stirring process was repeated three times, with the final stirring conducted overnight. The solution was then filtered through 0.45 μm filter membranes to yield a 4% sodium alginate working solution and stored at 4°C.

(ii) Gelatin working solution (15% [w/v]): Gelatin powder (Sigma-Aldrich, USA) was dissolved in the 0.9% NaCl solution. The solution was heated at 80°C for 3 h, followed by stirring at 750 rpm for 1 h at 37°C on a magnetic stirrer. The heating and stirring process was repeated three times. Then, the 15% gelatin working solution was stored at 4°C.

2.2. Polydimethylsiloxane user-defined micropatterning platform production and characterization

A silicon wafer was constructed with an inverted tetrahedron micropattern array as the original mold by wet-chemical etching. Polymethylmethacrylate (PMMA) hot pressing was performed on the silicon wafer using a hot press machine (WY-30T, Dongguan Weiying Machinery, China). PMMA was preheated at 150°C for 3 min, press-heated at 150°C and 500 psi for 10 min, and annealed while maintaining pressure. Different combinations of pressure (e.g., 300, 500, and 700 psi) and temperature (e.g., 100, 125, 150, and 175°C) were tested to determine the optimal parameters. The PMMA template was demolded mechanically from the silicon wafer. PDMS (DOWSIL, USA) was prepared by mixing the base component with the curing agent at a 10:1 (w/w) ratio. PDMS was cured on the PMMA template at 70°C for 80 min, forming the corresponding micropattern. Different curing times (e.g., 40, 60, 80, and 100 min) and temperatures (e.g., 60, 70, and 80°C) were tested to identify the optimal conditions. The PDMS micropatterns were then cut into circular inserts with a diameter of 1.5 mm and fitted into 24-well plates to form the PUMP system. The PUMP was sterilized before cell culture.

The stiffness of the PDMS was measured using uniaxial compression on a disk-shaped sample (1.3 mm thickness, 6 mm radius) prepared with the same composition as the PUMP, while a polystyrene sample served as a control, representing the AggreWell plate (STEMCELL Technologies, Canada).

The silicon wafer, PMMA stamp, and PDMS insert were coated with gold to enhance their electrical conductivity. Samples were imaged using a field emission scanning electron microscope (FE-SEM; JEOL JSM-7001, JEOL, Japan) with an accelerating voltage of 20.0 kV. The surface microstructure of the PDMS inserts was observed using a LEXT OLS4100 3D laser measuring microscope (Olympus, Japan), and microwell depth was measured.

2.3. Cell culture and differentiation on petri dishes, AggreWell plates, and polydimethylsiloxane user-defined micropatterning platform.

Human adipose-derived stem cell proliferation was performed by culturing hADSCs (Sciencell, USA) in mesenchymal stem cell medium (Sciencell, USA) in T75 culture flasks coated with 0.01 mg/mL poly-L-lysine solution (Sigma-Aldrich, USA) at 37°C in a humidified incubator with 5% CO_2. The medium was changed every 2 days. After the cells reached 90% confluence, the cells were digested using 0.25% trypsin-ethylenediaminetetraacetic acid (EDTA) (Gibco, USA) and passaged at a 1:3 ratio. In this study, hADSCs at passage four were used for subsequent experiments.

HUVEC proliferation was performed by culturing HUVECs (Peking Union Cell Resource Center, China) in endothelial basal medium-2 (EBM-2; LONZA, Switzerland) in T75 culture flasks at 37°C in a humidified incubator with 5% CO_2. The medium was changed daily. After the cells reached 90% confluence, the cells were digested using 0.25% trypsin-EDTA and passaged at a 1:2 ratio. HUVECs at passage four were used for subsequent experiments.

Differentiation of hICAs from hADSCs on petri dishes was performed by culturing hADSCs in hADSC–islet β-cell differentiation medium at a density of 1×10^5 cells/cm^2 for 5 days. The medium was changed every 2 days. PUMP inserts were coated with 1% Pluronic F127 (Sigma-Aldrich, USA), centrifuged at 3000 rpm for 5 min, and treated for 1 h. Then, hADSCs were seeded on treated PUMP inserts at densities of 0.8×10^5, 2.1×10^5, and 4.2×10^5 cells/cm^2 (equivalent to 200, 500, and 1000 cells per microwell, respectively) and centrifuged at 850 rpm for 3 min. Cells were cultured in hADSC–islet β-cell differentiation medium for 5 days, with half-medium changes every 2 days.

A parallel experiment was conducted on AggreWell plates using the same process. Cell densities were 1.2×10^5, 3.0×10^5, and 6.0×10^5 cells/cm^2, equivalent to 200, 500, and 1000 cells per microwell, respectively. The morphology and size of hICAs were monitored during the differentiation process. hICAs seeded at 4×10^5 cells/cm^2 on day 5 were collected for subsequent experiments.

All cells were observed and imaged using an optical microscope (Nikon, Japan). Image analysis was performed using ImageJ Pro 6.0 (National Institute of Health, USA).

2.4. Rheological testing of the bioinks

The bioinks were prepared by mixing gelatin working solution, sodium alginate working solution, Matrigel (Corning, USA), and DMEM to obtain a final concentration of 3.75% gelatin, 1% alginate, and 0.23% Matrigel, unless otherwise specified. The rheological properties were measured using a rotational rheometer (Anton Paar, Austria) with a cone-plate measuring sensor (diameter = 25 mm; cone angle = 1.99°; section = 99 μm). In oscillatory mode, the storage modules (G') and loss modulus (G") of uncrosslinked bioinks were recorded as functions of temperature at a strain of 0.1% and a frequency of 1 Hz. The temperature varied between 4 and 37°C at a rate of 2°C/min to replicate the heating and cooling process.

To further evaluate the rheological properties of crosslinked bioinks, the bioinks were crosslinked with 300 mM calcium chloride ($CaCl_2$; Sigma-Aldrich, USA) for 3 min, and the G' and G" were measured at a strain of 0.1% and a frequency of 1 Hz at 8, 15, and 22°C. In viscosity curve mode, the viscosity of uncrosslinked bioinks was measured over a shear rate scan range of 0.1–1000/s to assess shear-thinning properties.

2.5. Scanning electron microscopy of crosslinked bioinks

The crosslinked bioinks were lyophilized using a vacuum lyophilizer (Beijing Songyuanhuaxing Technology Development, China) for 3 days to maintain the microstructure, and then coated with gold to enhance their electrical conductivity. The samples were imaged using a FE-SEM operated at an accelerating voltage of 20.0 kV.

2.6. Three-dimensional bioprinting

For the 3D bioprinting of hICAs, the following procedure was performed. hICAs at day 5 in PUMP were harvested, centrifuged at 500 rpm for 1 min to collect aggregates, and resuspended in hADSC–islet β-cell differentiation medium at 6000 aggregates/mL (equivalent to 6×10^6 cells/mL). The hICA suspension was first mixed with the sodium alginate working solution at room temperature. The mixture was then combined with Matrigel on ice and incubated at 37°C for 5 min. Subsequently, the hICA–alginate–Matrigel mixture was mixed with the gelatin working solution to achieve a final bioink containing 3.75% gelatin, 1% alginate, and 0.23% Matrigel, with a cell aggregate density of 1200 aggregates/mL (equivalent to 1.2×10^6 cells/mL).

The hICA-laden bioink was printed using a 3D bioprinter (Regenovo Biotechnology Co., Ltd., China) with 25G needles (250 μm) onto 35-mm petri dishes precoated with 0.00125% poly-L-lysine under tri-module or dual-module thermal control. In tri-module bioprinting, the chamber was set to 8, 15, or 22°C, the printing nozzle was set to 1°C lower than the chamber, and the cooling plate was set to 12°C. Dual-module bioprinting used the same chamber and cooling plate temperature settings without nozzle temperature control. The printed six-layer structures were immediately crosslinked by adding 300 mM $CaCl_2$ for 3 min. The printed structures were cultured in hADSC–islet β-cell differentiation medium for 5 days, with the medium changed every 2 days.

For the 3D bioprinting of hICAs and HUVECs, the following steps were performed. HUVECs were harvested and resuspended at 4×10^6 cells/mL in EBM-2 medium. hICAs were harvested and centrifuged as described above, then resuspended at 12,000 aggregates/mL (equivalent to 1.2×10^7 cells/mL) in Hadsc–islet β-cell differentiation medium. After harvesting the hICAs from PUMP, several hICAs were picked and digested into single cells with 0.25% trypsin–EDTA to determine cell numbers. The hICA suspension and HUVEC suspension were then mixed at a 1:1 ratio to prepare the final cell suspension. The cell-laden bioink was prepared using the same method described above, with a final islet-like cell density of 1.2×10^6 cells/mL and HUVEC density of 4×10^5 cells/mL. The bioink was printed at 15°C using the same bioprinting method. The printed structures were cultured in a mixed medium composed of hADSC–islet β-cell differentiation medium and EBM-2 culture medium (1:1) for 5 days, with the medium changed every 2 days.

2.7. Live/dead staining

The live/dead staining solution contained 0.2% calcein–acetoxymethyl ester (Calcein-AM) and 0.3% propidium iodide (PI) (C542, Calcein-AM/PI Double Staining Kit, Donjindo, Japan) in phosphate-buffered saline (PBS). The cell-laden structures after bioprinting were incubated in the live/dead staining solution at room temperature for 10 min, followed by incubation in PBS for 10 min. The stained structures were then imaged using a confocal microscope (Nikon, Japan). As it was difficult to quantify cell numbers in aggregates, cell viability was evaluated by calculating the ratio of dead to live cell signal intensity from three different regions of the structures using the same imaging parameters.

2.8. Immunofluorescence staining

Immunofluorescence staining was performed on cells from planar differentiation, AggreWell plate differentiation, PUMP differentiation, and bioprinted structures on day 5. Primary antibodies included anti-PDX1 antibody (1:500; ab47383, Abcam, UK), anti-PAX6 antibody (1:50; ab5790, Abcam, UK), anti-Islet 1 (ISL1) antibody (1:200; ab86472, Abcam, UK), anti-INS antibody (1:50; ab7842, Abcam, UK), and anti-CD31 antibody (1:200; ab32457, Abcam, UK). The corresponding secondary antibodies

were used at a dilution of 1:1000, including donkey anti-goat IgG (ab150131, Abcam, UK), goat anti-mouse IgG (ab150077, Abcam, UK), goat anti-mouse IgG (ab150115, Abcam, UK), goat anti-guinea pig IgG (ab150185, Abcam, UK), and donkey anti-rabbit IgG (ab150073, Abcam, UK). Nuclei were stained with 4',6-diamidino-2-phenylindole (1 μg/mL; Invitrogen, USA).

The staining procedure was as follows: samples were washed with PBS for 5 min. Then, samples were fixed with 4% paraformaldehyde at 25°C for 30 min, or with 2.5% glutaraldehyde for 4 h if the cells were embedded in the printed structure, followed by washing with PBS for 5 min. Samples were permeabilized with 0.25% Triton X-100 (Sigma-Aldrich, USA) for 20 min, and washed with PBS for 5 min. Samples were then blocked with 10% bovine serum albumin (BSA; Multicell, USA) at 25°C for 1 h, and washed with PBS for 5 min. Subsequently, the samples were incubated with primary antibodies prepared in 0.3% Triton X-100 and 1% BSA overnight at 4°C, and washed with PBS for 5 min. Then, the samples were incubated with the corresponding secondary antibodies for 2 h in the dark and washed with PBS for 5 min. Finally, the samples were stained with 1 μg/mL of 4',6-diamidino-2-phenylindole at room temperature for 15 min in the dark, and washed with PBS for 5 min before imaging using a NIKON Z2 confocal microscope. ImageJ software was used for image processing and quantitative analysis.

2.9. Real-time fluorescence quantitative reverse transcriptase polymerase chain reaction

Quantitative reverse transcriptase polymerase chain reaction assay was performed on cells from planar differentiation, AggreWell plate differentiation, PUMP differentiation, and bioprinted structures on day 5. Samples were washed with PBS for 5 min. Cells in the bioprinted structures were harvested by degrading the construct using a hydration solution (150 mM NaCl, 55 mM sodium citrate, and 20 mM EDTA) for 3 min, followed by termination with culture medium. The cells were lysed using TRIzol (Ambion, USA). For every 1 mL of TRIzol, 0.2 mL trichloromethane was added, the samples were thoroughly mixed, and incubated at room temperature for 10 min. The samples were centrifuged at 13,500 rpm at 4°C for 15 min. The upper aqueous phase was collected and mixed with an equal volume of isopropyl alcohol. The mixture was incubated on ice for 10 min. Then, the samples were centrifuged at 13,500 rpm at 4°C for 8 min, and the supernatant was removed. The RNA pellet was washed with 75% ethanol prepared in RNase-free double-distilled water.

Subsequently, the samples were centrifuged at 10,600 rpm at 4°C for 5 min, and the supernatant was removed. RNase-free double-distilled water was added to dissolve the RNA on ice. RNA concentration was measured using a NanoDrop 2000 spectrophotometer (Thermo Scientific, USA). Based on the RNA concentration and according to the manufacturer's instructions for the FastKing RT Kit (with gDNase) (TIANGEN Biotech, China), RNA reverse transcription was performed using a thermal cycler (T960, Heal Force, China). cDNA amplification was performed according to the manufacturer's instructions for the SuperReal PreMix Plus (SYBR Green) kit (TIANGEN Biotech, China). A real-time fluorescence quantitative polymerase chain reaction system (CFX96, Bio-Rad, USA) was used for signal detection. The primer sequences are listed in Table 1.

2.10. Glucose-stimulated insulin secretion assay

The INS secretion function of hICAs was assessed using a GSIS assay. Bioprinted structures were degraded using a hydration solution, and cell aggregates were harvested. The cell aggregates, hICAs or hIOs, were washed with PBS at least once, and then incubated in Krebs–Ringer bicarbonate buffer without glucose (10 mM 4-(2-hydroxyethyl)piperazine-1-ethanesulfonic acid, 25 mM sodium bicarbonate, 120 mM NaCl, 5 mM potassium chloride, 2.5 mM $CaCl_2$, 1.1 mM magnesium chloride, and 0.1% BSA) for 6 h. Cell aggregates were then incubated with Krebs–Ringer bicarbonate buffer containing 2.8 mM glucose for 1 h, followed by incubation with 16.7 mM glucose for 1 h. The supernatants from these two stages were collected separately. INS concentration was measured using a human INS enzyme-linked immunosorbent assay kit (SEKH-0219, Solarbio, China) according to the manufacturer's instructions. The ratio of INS content secreted at 16.7 mM glucose to that at 2.8 mM glucose was defined as the glucose stimulation index.

2.11. Statistical analysis

Data are presented as mean ± standard deviation or as range for quantitative analyses. The Statistical Package for Social Sciences version 24.0 (IBM, USA) was used to perform two-sided Student's *t*-tests, one-way analysis of variance (ANOVA), and two-way ANOVA with Bonferroni's multiple comparison test. A p-value < 0.05 was considered statistically significant.

3. Results and discussion

3.1. Fabrication and characterization of the polydimethylsiloxane user-defined micropatterning platform system

Pancreatic islets are clusters of cells that function more efficiently under 3D aggregation conditions. The formation of aggregates using micropatterning technology has become

Table 1. Primer sequences of tested genes

Primer	Forward sequence (5'–3')	Reverse sequence (3'–5')
CD31	AAGTGGAGTCCAGCCGCATATC	ATGGAGCAGGACAGGTTCAGTC
CD73	CTGATGATGGGCGGAAGGTT	ATCAATGGGCGACCGGATAC
CDH5	GAAGCCTCTGATTGGCACAGTG	TTTTGTGACTCGGAAGAACTGGC
HES1	GGAAATGACAGTGAAGCACCTCC	GAAGCGGGTCACCTCGTTCATG
INS	ACGAGGCTTCTTCTACACACCC	TCCACAATGCCACGCTTCTGCA
ISL1	GCAGAGTGACATAGATCAGCCTG	GCCTCAATAGGACTGGCTACCA
KDR	GGAACCTCACTATCCGCAGAGT	CCAAGTTCGTCTTTTCCTGGGC
NGN3	CCTAAGAGCGAGTTGGCACTGA	AGTGCCGAGTTGAGGTTGTGCA
NKX6-1	CCTATTCGTTGGGGATGACAGAG	TCTGTCTCCGAGTCCTGCTTCT
NOS3	GAAGGCGACAATCCTGTATGGC	TGTTCGAGGGACACCACGTCAT
PDX1	GAAGTCTACCAAAGCTCACGCG	GGAACTCCTTCTCCAGCTCTAG
SOX9	AGGAAGCTCGCGGACCAGTAC	GGTGGTCCTTCTTGTGCTGCAC
VWF	CCTTGAATCCCAGTGACCCTGA	GGTTCCGAGATGTCCTCCACAT
GAPDH	GTCTCCTCTGACTTCAACAGCG	ACCACCCTGTTGCTGTAGCCAA

Abbreviations: CD31, platelet endothelial cell adhesion molecule 1 gene (*PECAM1*); *CD73*, 5'-nucleotidase Ecto gene (*NT5E)*; *CDH5*, cadherin 5 gene; *GAPDH*, glyceraldehyde-3-phosphate dehydrogenase gene; *HES1*, Hes Family BHLH transcription factor 1 gene; *INS*, insulin gene; *ISL1*, islet 1 gene; *KDR*, kinase insert domain receptor gene; *NGN3*, neurogenin-3 gene; *NKX6-1*, NK6 homeobox 1 gene; *NOS3*, nitric oxide synthase 3 gene; *PDX1*, pancreatic and duodenal homeobox 1 gene; *SOX9*, SRY-box transcription factor 9 gene; *VWF*, von Willebrand factor gene.

a popular method due to its efficiency in producing large quantities of uniform cell aggregates.[18] Previous studies have shown that the geometry of microwells significantly influences the morphology of these aggregates, with V-shaped microwells promoting the formation of more uniform and compact structures.[19] Among the commercially available platforms, the AggreWell plate is a widely recognized V-shaped microwell array. However, it has several limitations, including fixed shapes, excessive substrate stiffness, high costs, and limited reusability. These challenges may hinder its versatility and reduce its appeal for diverse applications.

To address these challenges, we developed the PUMP system, which enables customization of microwell size, shape, and stiffness to meet various cell aggregation requirements. The PUMP fabrication process involved anisotropic wet etching of silicon wafers, hot pressing of PMMA, and curing and insertion of PDMS. This resulted in an inverted pyramid-shaped, V-angled PDMS micropatterning array (Figure 2A).

The dimensions of the micropatterns on the silicon wafer were determined by the mask design and etching parameters. To ensure accurate reproduction of the micropatterns, we assessed the processing conditions for PMMA hot pressing (Figure 2B) and PDMS curing (Figure 2C) to identify the optimal parameter combinations, indicated by gray circles. Using a square mask pattern with a side length of 490 μm and a spacing of 10 μm, we successfully produced densely packed V-shaped microwells with a side length of approximately 485 μm and a depth of about 352 μm, closely matching the intended geometry (Figure 2D & E).

Scanning electron microscopy and laser confocal scanning confirmed that fine structural features were preserved at both the tips and bases of the micropatterns throughout the manufacturing process, with a final tip angle of 70° replicating that of the silicon template (Figure 2D). To facilitate cell seeding and culture, the PDMS micropatterns were punched into cylindrical inserts with diameters of 1.1, 1.5, 2.3, and 3.4 cm, which fit into 48-well, 24-well, 12-well, and 6-well plates, resulting in approximately 400, 740, 1740, and 3810 micropatterns in each well, respectively. This method ensures reproducibility and versatility in the fabrication process, effectively preventing mold adhesion and topographic deformation, which are commonly associated with traditional PDMS casting techniques.[20]

Unlike the AggreWell plate, the PUMP substrate is composed of PDMS, a biocompatible elastomeric material. To evaluate its mechanical compliance, we conducted uniaxial compression tests to measure the Young's modulus of PDMS samples. In contrast to the rigid polystyrene substrate used in AggreWell plates, which has a Young's modulus of approximately 2.6 GPa, the PDMS in the PUMP system exhibited a significantly lower stiffness of approximately 2.0 MPa (Figure 2F). This

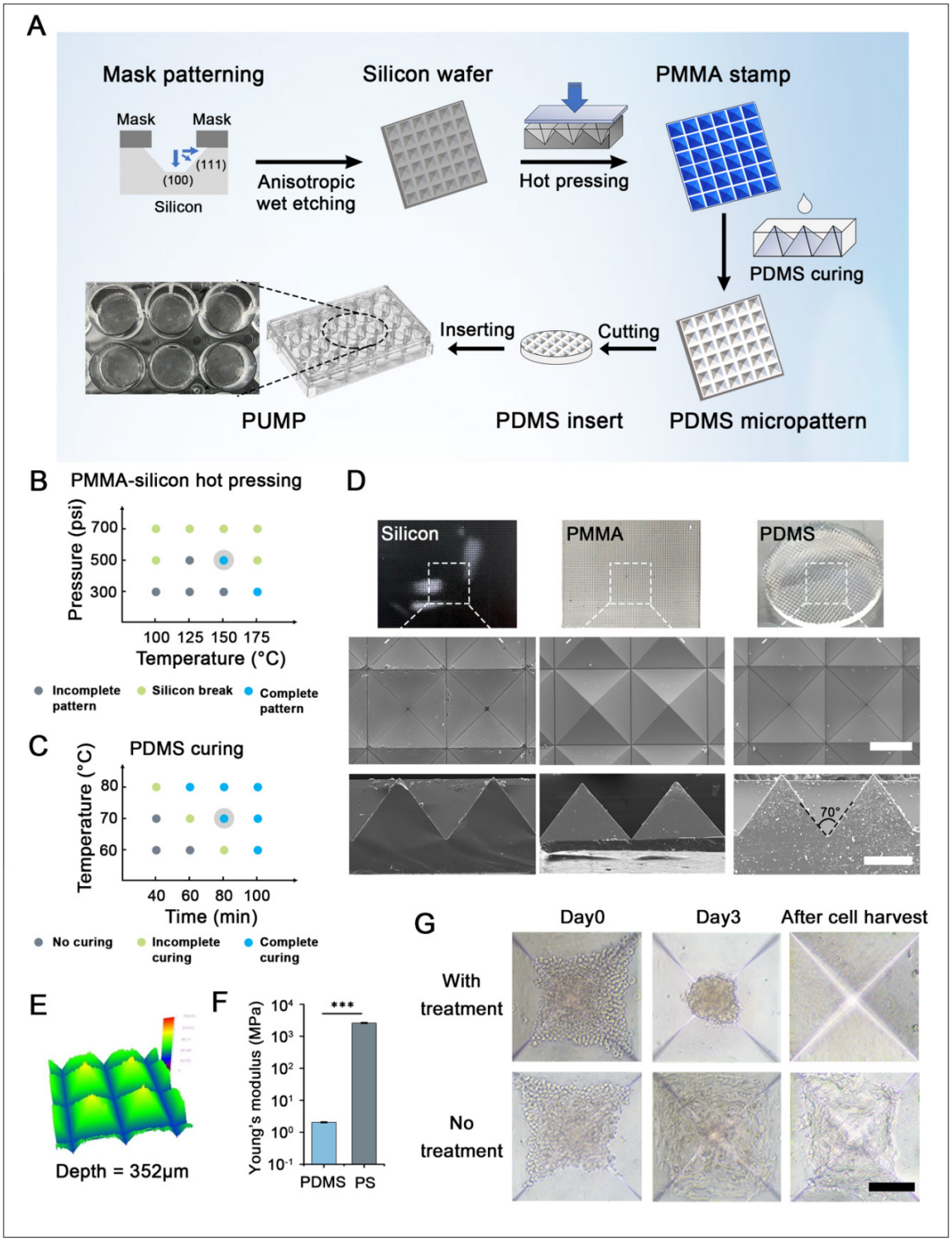

Figure 2. Fabrication and characterization of the PUMP system. (A) Schematic illustration of the fabrication process of the PUMP system. (B, C) Optimization of processing parameters for PMMA hot pressing (B) and PDMS curing (C), with grey circles indicating the optimized conditions used in subsequent experiments. (D) Macroscopic and scanning electron microscopy images of the silicon wafer, PMMA stamp, and PDMS micropattern (scale bar: 250 μm; magnification: 100×). (E) Quantitative analysis of PUMP microwell depth using a laser confocal scanning microscope. (F) Comparison of the Young's modulus of PDMS and PS, representing the substrate materials of the PUMP and AggreWell plates, respectively. (G) Representative images of human adipose-derived mesenchymal stem cells seeded and cultured in PUMP with and without Pluronic F127 treatment (scale bar: 150 μm; magnification: 100×). Statistical analysis was conducted using a two-sided Student's *t*-test. Triple asterisk (***) indicates statistical significance at $p < 0.001$. Abbreviations: PDMS, polydimethylsiloxane; PMMA, polymethylmethacrylate; PUMP, polydimethylsiloxane user-defined micropatterning platform; PS, polystyrene.

substantial reduction in stiffness, by nearly three orders of magnitude, may help minimize stress-induced cellular effects during culture.[21]

To assess cell clustering performance, we cultured hADSCs in the PUMP using a proliferative medium. With proper treatment using Pluronic F127, cell adhesion to the PUMP substrate was effectively prevented, allowing the rapid formation (within 24 h) of cell aggregates with smooth and well-defined contours. These aggregates can be easily harvested through gentle pipetting, leaving no detectable cell residues behind (Figure 2G). Additionally, the PUMP system demonstrated excellent reusability. A PMMA stamp can be reused for at least 50 fabrication cycles, while each PDMS insert can be reused four to five times without compromising cell aggregation efficiency or harvesting performance. This high durability highlights the economic advantages of the PUMP system for repeated applications.

In summary, the PUMP system provides a cost-effective, reusable, and highly customizable platform with user-defined micropatterning geometries and significantly reduced stiffness compared to commercial micropatterning systems. Collectively, these attributes make it a versatile tool for a wide range of cell culture and aggregation applications.

3.2. Large-scale generation of human islet β-like cell aggregates

hADSCs are a type of mesenchymal stem cell derived from human adipose tissue. Previous studies have shown that these cells exhibit strong proliferative capabilities and the potential to differentiate into various cell types, including islet-like cells.[9,22] Due to their accessibility through procedures such as liposuction or surgical fat excision, hADSCs are considered a promising source for autologous tissue engineering and broad clinical applications.

To evaluate the differentiation capacity of hADSCs, we conducted planar differentiation to generate islet β-like cells following an established protocol.[10] Over a 5-day differentiation period, we observed the formation of compact cell clusters with irregular shapes and considerable size variability (Figure 3A). The differentiated hADSCs expressed islet-related marker proteins, including PDX1, PAX6, ISL1, and INS (Figure 3B). Furthermore, the expression levels of islet-related marker genes—*PDX1*, *NGN3*, *ISL1*, *NKX6-1*, and *INS*—were upregulated by 2.8-fold, 6.1-fold, 7.3-fold, 1.8-fold, and 2.8-fold, respectively, with statistically significant differences compared to undifferentiated hADSCs (Figure 3C). These results confirm the ability of hADSCs to differentiate into a pancreatic islet β-cell lineage, consistent with previous studies.[9,22]

Additionally, we conducted islet β-cell differentiation of hADSCs within the PUMP system using the same differentiation cytokines as in planar culture, with AggreWell as a parallel control. To obtain cell aggregates of uniform and appropriate size, different cell seeding densities were tested, including 0.8×10^5, 2.1×10^5, and 4.2×10^5 cells/cm^2 (equivalent to 200, 500, and 1000 cells per microwell). From day 1, cells at all seeding densities rapidly formed tight clusters with smooth contours and showed no adhesion to the substrates in either system (Figure 4A). Throughout the 5-day culture period, both systems maintained relatively stable aggregate sizes, and no significant differences were observed in the aggregates formed from 500 and 1000 cells between the PUMP and AggreWell plates (Figure 4B & C).

Moreover, the size of cell aggregates on day 5 demonstrated a positive correlation with the initial cell seeding density. The cell aggregates had diameters of 92.8 ± 10.5 μm, 114.8 ± 12.6 μm, and 132.8 ± 10.4 μm, at initial cell seeding densities of 200, 500, and 1000 cells per microwell, respectively (Figure 4B). The diameters of hICAs derived from the PUMP system with 1000 cells per microwell were mainly between 120 and 140 μm, closely resembling the average islet diameter *in vivo* (approximately 120 μm). Thus, we selected a seeding density of 1000 cells per microwell, achieving large-scale production of approximately 15,000 hICAs per 24-well plate (Figure 4D). The size uniformity of the PUMP system is comparable to that of the AggreWell plates and is significantly improved compared with planar differentiation (Figure 4E). Furthermore, the aggregates in both the PUMP and AggreWell plates exhibited high viability (Figure 4F).

The findings revealed that hICAs from PUMP expressed islet-related markers, including *PDX1*, *PAX6*, *ISL1*, and *INS* (Figure 4G). The expression of *PDX1*, *NKX6-1*, *INS*, and the hADSC-specific gene *CD73* was quantitatively evaluated (Figure 4H). The expressions of *PDX1*, *NKX6-1*, and *INS* were upregulated by 1.22-fold, 1.23-fold, and 3.05-fold, respectively, with statistical significance compared to planar culture. In contrast, the expression of *CD73* was downregulated to 0.83-fold. When compared with AggreWell plates, the expression of *ISL1* and *NKX6-1* was upregulated by 2.67-fold and 1.33-fold, respectively, with statistical significance. However, the expression of *CD73* was downregulated to 0.72-fold (Figure 4I). These results indicate that the PUMP system facilitated islet β-cell differentiation of hADSCs more effectively than planar culture. This may be due to the PUMP system establishing a physiology-related culture environment compared to planar differentiation, where limited cell–cell interactions lead to proliferation inhibition rather than complex interactions. In addition, the PUMP also exhibited better

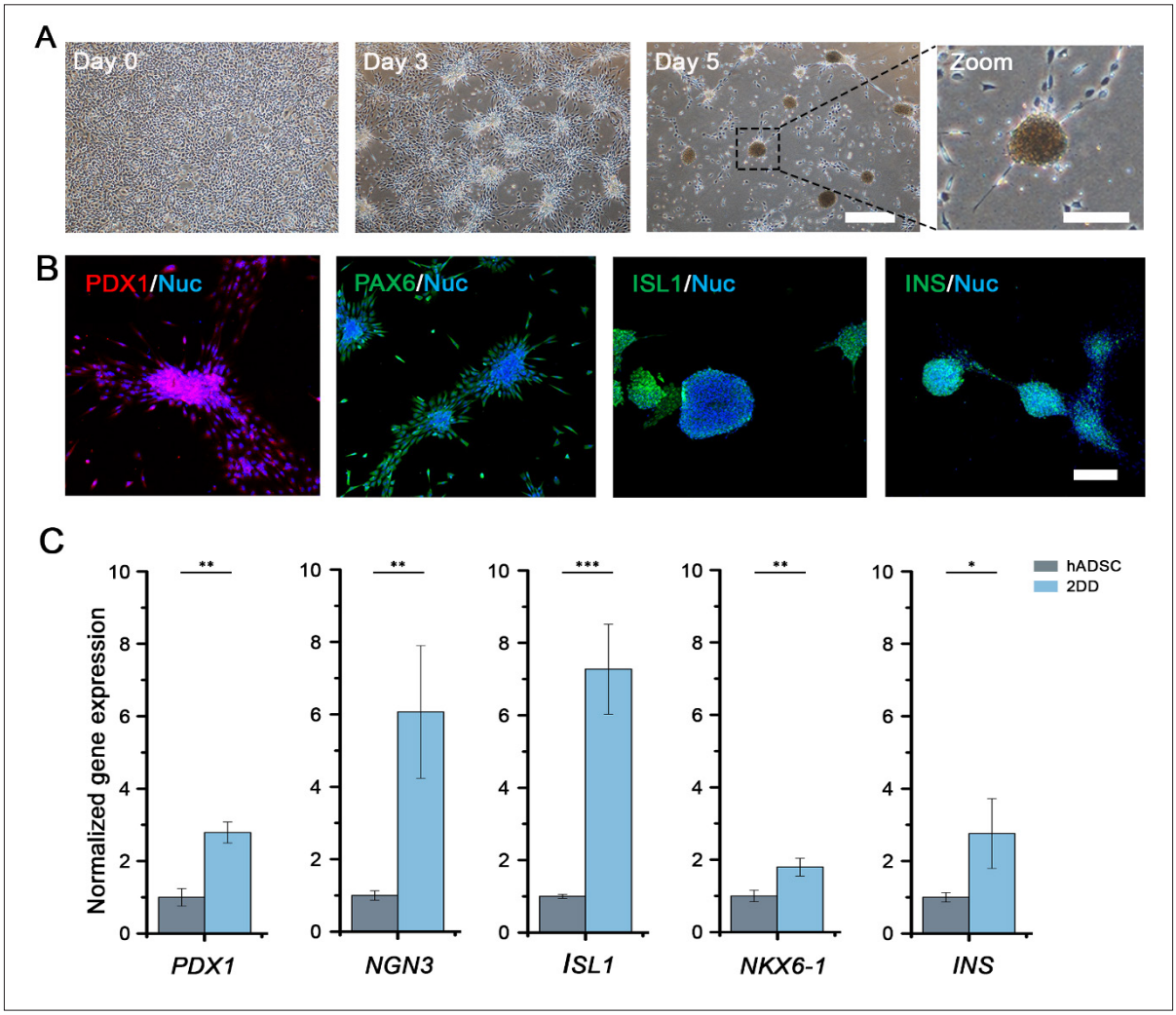

Figure 3. Planar differentiation of hADSCs into islet β-like cells. (A) Phase-contrast microscopy images during the 5-day planar differentiation process (scale bar: 500 μm; magnification:40×). (B) Immunofluorescence images of the cells after 5 days of planar differentiation (scale bar: 200 μm; magnification: 100×). (C) Relative gene expression of cells before (hADSCs) and after planar differentiation (2DD). Gene expression levels were normalized to hADSCs and are represented as $2^{-\Delta\Delta Ct}$ ($n = 3$). Statistical analysis was conducted using a two-sided Student's *t*-test. Single asterisk (*), double asterisk (**), and triple asterisk (***) indicate statistical significance at $p < 0.05$, $p < 0.01$, and $p < 0.001$, respectively. Abbreviations: 2DD, two-dimensional differentiation; hADSC, human adipose-derived mesenchymal stem cell; INS, insulin; ISL1, islet 1; NGN3, neurogenin-3; NKX6-1, NK6 homeobox 1; PAX6, paired box gene 6; PDX1, pancreatic and duodenal homeobox 1.

functionality in differentiating into the islet β-cell lineage compared with commercial AggreWell plates.

Taken together, these results demonstrate that the PUMP system can promote differentiation into hICAs more effectively compared with both planar differentiation and AggreWell plates. Although planar differentiation provides greater exposure of cells to soluble chemical factors, the uniform aggregate structure formed in the PUMP system may contribute to higher expression of islet-related genes. The improvement in hICAs' maturity from PUMP may be partially attributed to the lower stiffness of the culture environment. It has been reported that a high-stiffness environment can reduce *INS* expression,[23] and substrates with stiffness similar to that of the pancreas can help *in vitro* islet-like cells recapitulate the *in vivo* functions of islets.[24] In all, hICAs can be harvested from PUMP with uniform sizes and enhanced differentiation at a large scale, thereby satisfying the requirements for 3D bioprinting and the fabrication of hIOs in subsequent applications.

3.3. Optimization of tri-module bioprinting with ternary bioinks for aggregate bioprinting

A 3D culture environment provides structural, physical, and chemical cues for encapsulated aggregates, which are crucial for further differentiation and maturation.[25,26]

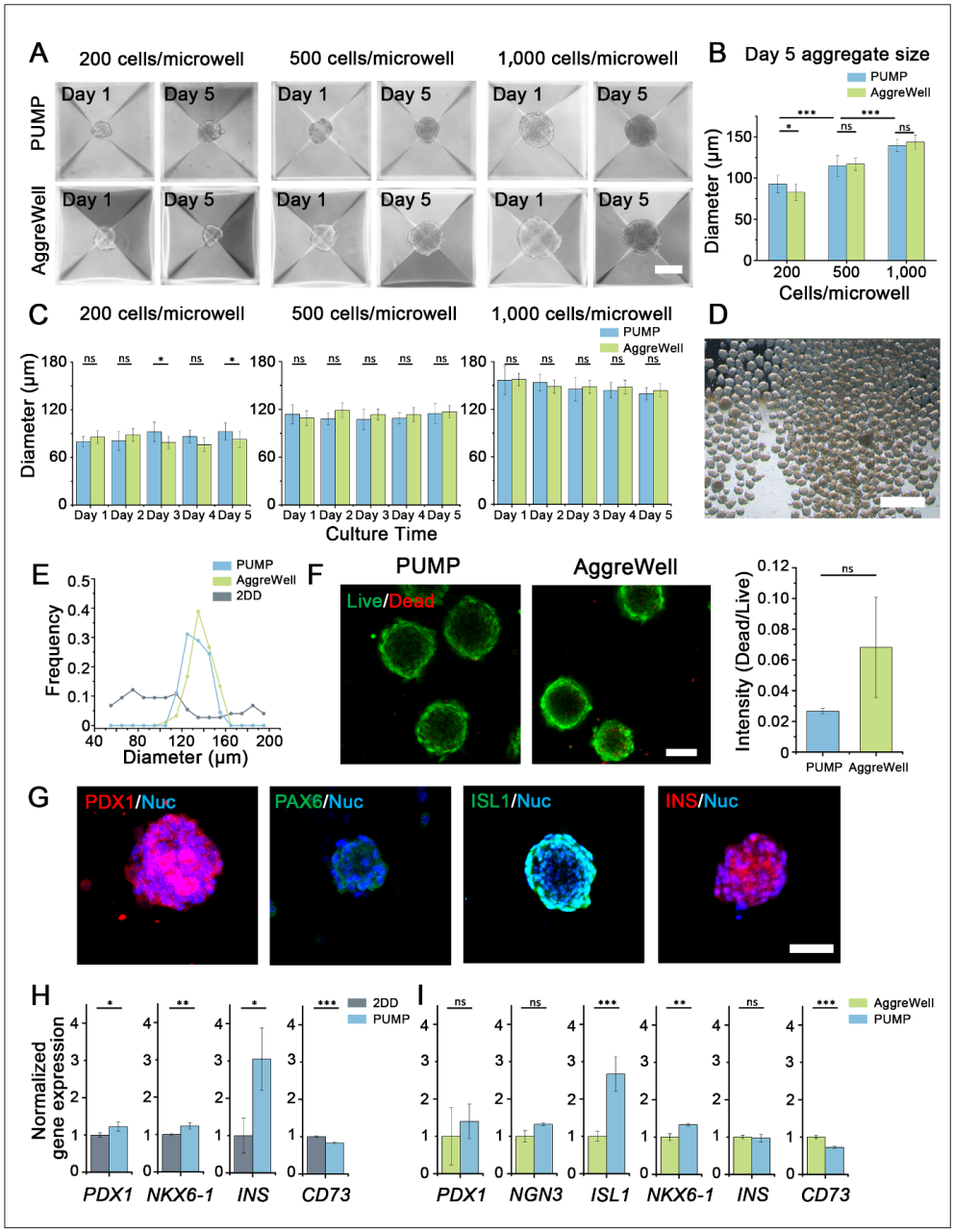

Figure 4. Generation and biological characterization of hICAs in PUMP. (A) Phase-contrast microscopy images of aggregates cultured in PUMP and AggreWell plates with 200, 500, or 1000 cells per microwell (scale bar: 100 μM; magnification: 100×). (B) Aggregate size in PUMP or AggreWell plates with 200, 500, and 1000 cells per microwell on day 5. (C) Changes in aggregate diameter during the 5-day differentiation in PUMP and AggreWell plates at 200, 500, and 1000 cells per microwell. (D) Morphology of hICAs harvested from PUMP on day 5 (scale bar: 500 μM; magnification: 40×). (E) Size distribution of aggregates generated from PUMP, AggreWell plates, and planar differentiation (2DD). (F) Viability assay of aggregates with 1000 cells per microwell on day 5 (scale bar: 50 μM; magnification: 200×). (G) Immunofluorescence images of differentiated cells expressing islet-related markers (PDX1, PAX6, ISL1, and INS) in hICAs derived from PUMP (scale bar: 50 μM; magnification: 200×). (H) Relative gene expression of islet-related markers (*PDX1*, *NKX6-1*, and *INS*) and the hADSC marker (*CD73*) in hICAs differentiated under planar culture (2DD) and PUMP. Gene expression levels were normalized to 2DD and presented as $2^{-\Delta\Delta Ct}$ ($n = 3$). (I) Relative gene expression of islet-related markers (*PDX1*, *NGN3*, *ISL1*, *NKX6-1*, and *INS*) and the hADSC marker (*CD73*) in hICAs differentiated using AggreWell plates and PUMP. Gene expression levels were normalized to AggreWell plates and presented as $2^{-\Delta\Delta Ct}$ ($n = 3$). Statistical analysis was conducted using two-way ANOVA with Bonferroni's multiple comparisons test (B and C) or two-sided Student's *t*-test (F, H, and I). Single asterisk (*), double asterisk (**), and triple asterisk (***) indicate statistical significance at $p < 0.05$, $p < 0.01$, and $p < 0.001$, respectively. "ns" denotes no statistical significance. Abbreviations: 2DD, two-dimensional differentiation; CD73, 5'-nucleotidase Ecto gene (*NT5E*); hADSC, human adipose-derived mesenchymal stem cell; hICA, human islet β-like cell aggregate; INS, insulin; ISL1, islet 1; NGN3, neurogenin-3; NKX6-1, NK6 homeobox 1; PAX6, paired box gene 6; PDX1, pancreatic and duodenal homeobox 1; PUMP, polydimethylsiloxane user-defined micropatterning platform.

However, given the avascular nature of hydrogels and aggregates, nutrient and oxygen diffusion can be a significant issue in supporting cell survival and function.[27] Therefore, we bioprinted hICA-embedded porous bioinks into a mesh structure (Figure 5A), where the spacing between filaments and the micropores within the bioinks may be compatible with long-range and short-range diffusion, respectively.

In addition to printability and biocompatibility, bioinks used for aggregate bioprinting require careful consideration of additional factors, including nozzle clogging, aggregate damage during printing, and the need for appropriate mechanical properties and mass transfer characteristics after printing. In this study, we developed a ternary bioink composed of gelatin, alginate, and Matrigel. In our previous work, a foundational combination of 3.75% gelatin and 1% alginate demonstrated good printability.[28,29] We further introduced Matrigel into the bioinks to mimic the extracellular matrix surrounding pancreatic islets[30] and to enhance the differentiation of pancreatic progenitor cells.[31] However, within the temperature range of 4–37°C, Matrigel accelerates crosslinking as the temperature increases, lacking a precise temperature transition point, which thereby increases the instability of the printing process.

In our preliminary experiment, diluted Matrigel at final concentrations of 0.08% and 0.23% remained uncrosslinked, whereas 0.4% Matrigel showed flocculation and uneven material distribution (Figure 5B). Thus, we adopted a composition of 3.75% gelatin, 1% alginate, and 0.23% Matrigel for the final bioink formulation, ensuring the highest possible biological content. The bioinks exhibited distinct rheological properties during the cooling and heating processes (Figure 5C). The gelling temperatures during cooling and heating were approximately 15 and 25°C, respectively. This indicates that the bioinks are printable with rapid solidification below 15°C, and that the printed structures remain temporarily stable under temperature fluctuations up to 25°C. Bioinks cooled to 8, 15, and 22°C exhibited shear-thinning properties, which is beneficial for bioprinting aggregates due to their reduced viscosity (Figure 5D). With subsequent alginate crosslinking, the bioinks crosslinked at 15°C exhibited a long-term shear storage modulus of 929 Pa and a loss modulus of 259 Pa, values that fall within the range of the healthy human pancreas (Figure 5E).[32] On the other hand, the bioinks crosslinked at 8°C showed a higher storage modulus than pancreatic tissue, while those at 22°C failed to crosslink.

Considering the temperature sensitivity of the bioinks during bioprinting, we developed a tri-module bioprinting strategy that allowed independent control of the printing chamber, printing nozzle, and cooling plate temperatures. At a chamber temperature of 15°C, the printed bioink maintained an intact mesh structure, both with and without cell aggregates. At 8°C, the printed bioink was over-crosslinked, resulting in broken and thinner filaments, whereas at 22°C, it was under-crosslinked and failed to form stable structures (Figure 5F). Therefore, 15°C was selected as the optimal temperature for the chamber. No significant change in filament width was observed after culturing the structures for 7 days, indicating the long-term stability of the bioprinted constructs (Figure 5G). SEM of the crosslinked bioink revealed a pore size of 49.4 μm, sufficient to allow cell migration and promote local mass transfer (Figure 5H). By optimizing both the bioink formulation and the printing parameters, we achieved suitable constructs for aggregate bioprinting, with composition and stiffness comparable to those of native pancreas tissues.

When applied to aggregate bioprinting, we initially observed heterogeneous aggregate distribution across different bioprinted structures (Figure 6A). This is because, before the bioink was extruded, its crosslinking status was not controlled without a well-defined nozzle temperature. As a result, the movement of aggregates was affected. Thus, we developed a tri-module bioprinting strategy with specific nozzle temperature control, achieving homogeneous aggregate distribution and high viability among 20 different structures during a single bioprinting process (Figure 6A & B).

3.4. Maintenance of islet-related marker expression in bioprinted human islet β-like cell aggregates

Based on the optimized ternary bioink composition and tri-module bioprinting strategy, we bioprinted the hICAs and evaluated their morphology and islet-related marker expression (Figure 7A). By day 5, obvious cell spreading was observed from hICAs, in contrast to the compact aggregates present on day 0 (Figure 7B). Immunofluorescence staining showed that hICAs remained positive for islet-related markers after 5 days of culture within the bioprinted structures, including *PDX1*, *PAX6*, *ISL1*, and *INS* (Figure 7C).

These findings suggest that our optimized bioinks provided a biomimetic extracellular matrix that supported the attachment and differentiation of hICA. However, the strong matrix–cell interaction also induced the disassembly of several aggregates, indicating a lack of intercellular signaling necessary to maintain hICA's structural integrity. In this study, hICAs did not include endothelial cells, as differentiation was restricted to the endocrine β-lineage from hADSCs. This highlights the

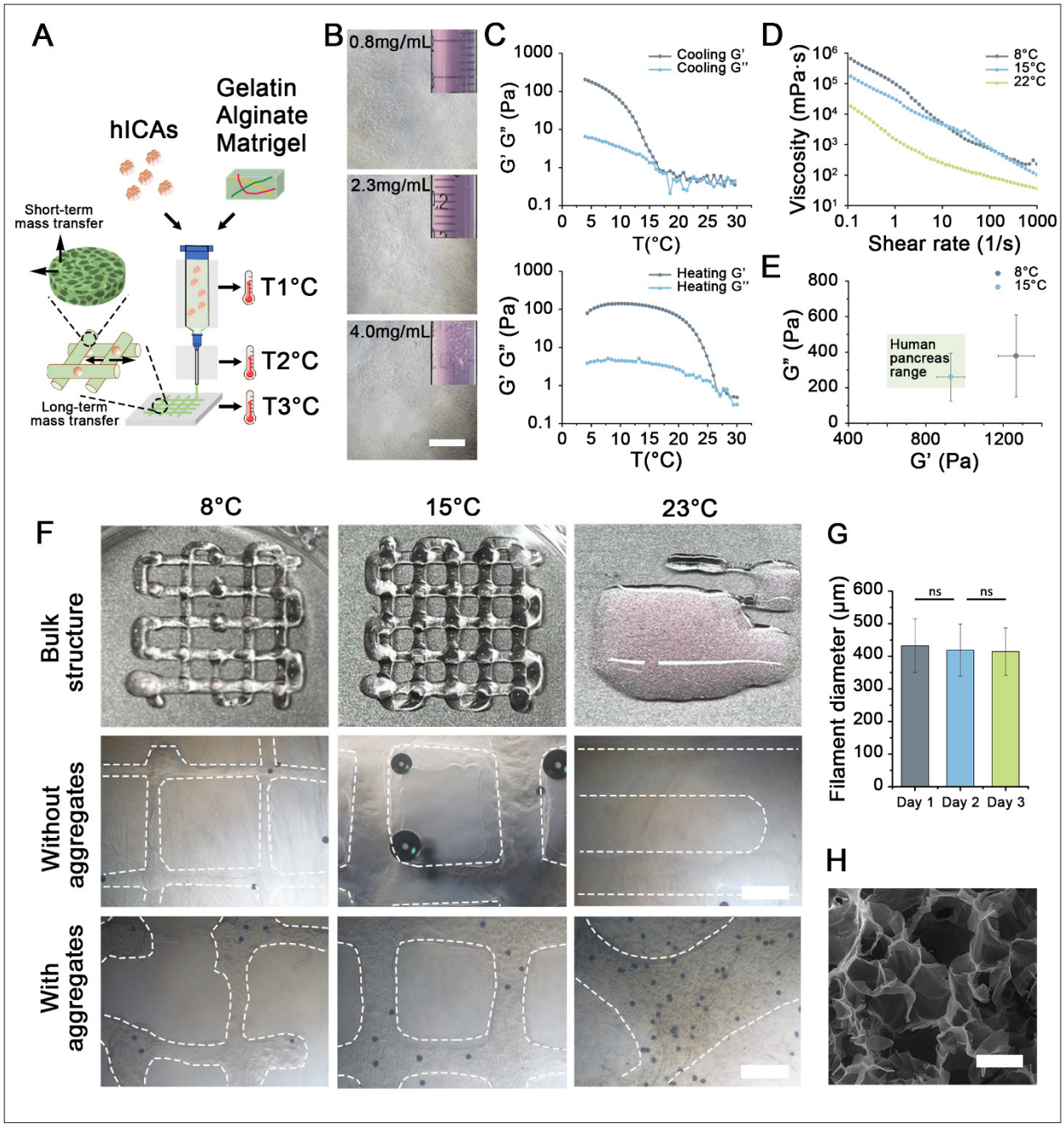

Figure 5. Rheological and structural characterization of bioinks to improve printability. (A) Schematic illustration of the tri-module thermal control strategy for bioprinting, based on the rheological properties of the bioinks. (B) Micro- and macro-scale images (top-right: Matrigel in syringes) of bioinks containing different concentrations of Matrigel (scale bar: 200 μm; magnification: 100×). (C) Shear storage modulus (G') and loss modulus (G") of bioinks measured at 0.1% strain and 1 Hz, during temperature decrease or increase at 2°C/min. (D) Viscosity profiles of bioinks at different temperatures as a function of shear rate. (E) Storage and loss moduli (G' and G") of bioinks after crosslinking with calcium chloride at 8 and 15°C, measured at 0.1% strain and 1 Hz, and compared with those of healthy human pancreatic tissue. (F) Bulk structural images (row 1), microscopic images without cell aggregates (row 2), and microscopic images with cell aggregates (row 3) of printed constructs at 8°C (over-crosslinked), 15°C (properly crosslinked), and 22°C (under-crosslinked) (scale bar: 500 μm; magnification: 40×). (G) Filament diameter changes of printed constructs during 7 days of culture. (H) Scanning electron microscopy images showing internal pore morphology of bioinks after proper crosslinking (scale bar: 50 μm; magnification: 500×). Statistical analysis was performed using one-way analysis of variance with Bonferroni's multiple comparisons test. "ns" denotes no statistical significance. Abbreviations: hICA, human islet β-like cell aggregate; T, temperature.

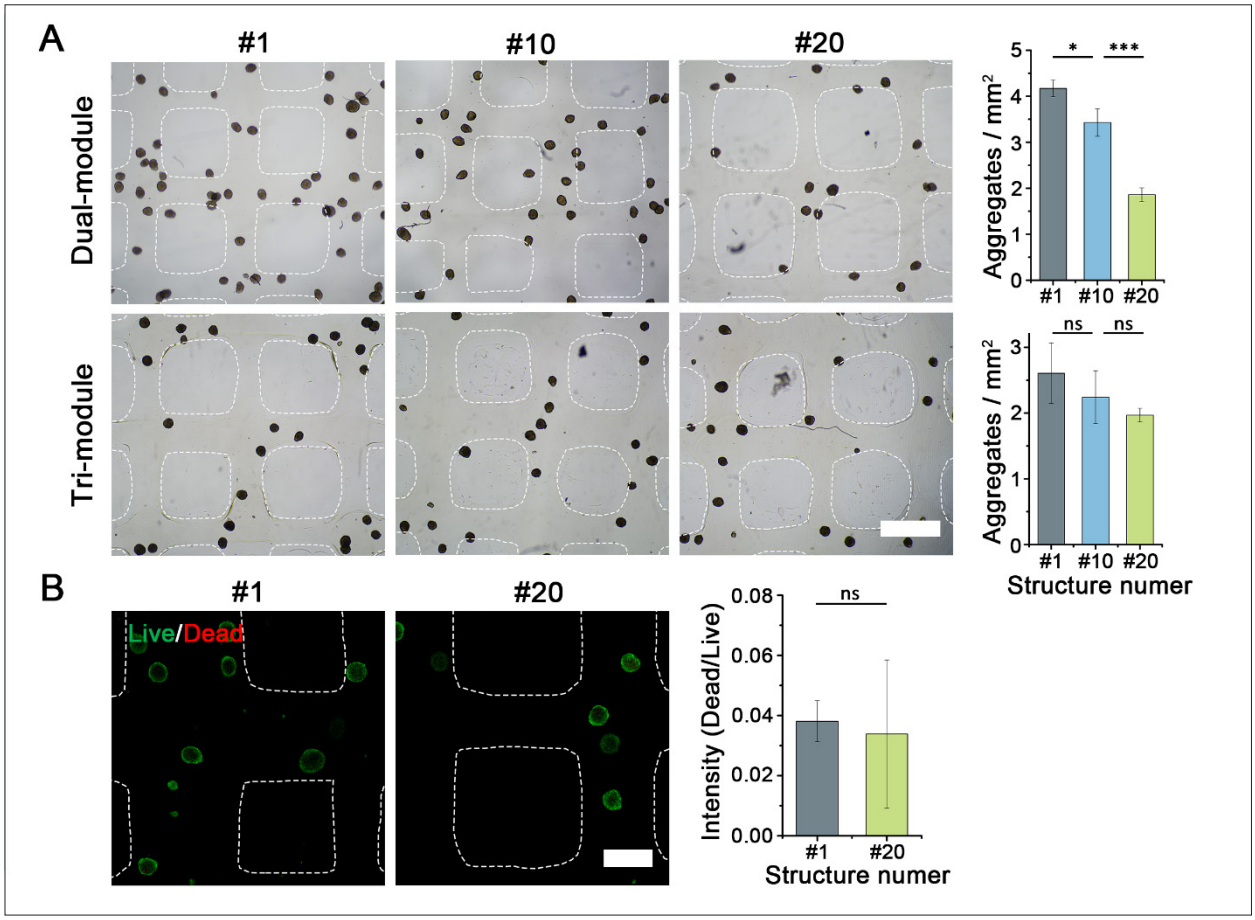

Figure 6. Printing performance of the three-dimensional bioprinting system with dual-module or tri-module thermal control. (A) Aggregate density changes in printed structures from the first sample (#1) to the 20th sample (#20) using traditional dual-module or tri-module thermal control, with quantitative analysis (scale bar: 1 mm; magnification: 20×). (B) Live/dead staining images of aggregates in all bioprinted structures produced under tri-module thermal control, with semi-quantitative analysis (scale bar: 500 μm; magnification: 40×). Statistical analysis was performed using one-way analysis of variance with Bonferroni's multiple comparisons test (A) or two-sided Student's *t*-test (B). Single asterisk (*) and triple asterisk (***) indicate statistical significance at $p < 0.05$ and $p < 0.001$, respectively. "ns" denotes no statistical significance.

potential of incorporating multiple cell types to construct vascularized islet organoids, thereby promoting the further maturation of hICAs.

3.5. Production of vascularized human islet organoid by self-assembly of human islet β-like cell aggregates and human umbilical vein endothelial cells

In vivo, endothelial cells not only form blood vessels,[33] but also promote the differentiation of progenitor cells into endocrine cells and support islet maturation.[34] Recent studies have also shown that endothelial cells play a crucial role in promoting the maturation of pancreatic progenitor cells.[35–37] Therefore, we bioprinted hICAs with HUVECs to further promote the self-assembly of hIOs (Figure 7E).

Both hICAs and HUVECs exhibited viability exceeding 90% after printing (Figure 7D). On day 0, the aggregates (hICAs) and single cells (HUVECs) were separated from each other, as they were homogeneously distributed in the bioinks. By day 3, several single cells appeared around the aggregates, and by day 5, their number further increased. From day 0 to day 5, we observed obvious recruitment of single cells to the surface of the aggregates, suggesting self-assembly driven by intercellular communication through paracrine signaling and HUVEC migration (Figure 7D).

On day 5, immunofluorescence staining further showed that HUVECs formed a tight layer encapsulating individual hICAs, rather than forming vascular connections among aggregates (Figure 7E). The co-culture enhanced the structural integrity of hICAs within the printed hydrogel. The recruitment of HUVECs to the surface of hICAs also mimics the process during pancreatic development, in which endothelial cells migrate to endocrine cell aggregates.[38] The elongated endothelial cell layer structure

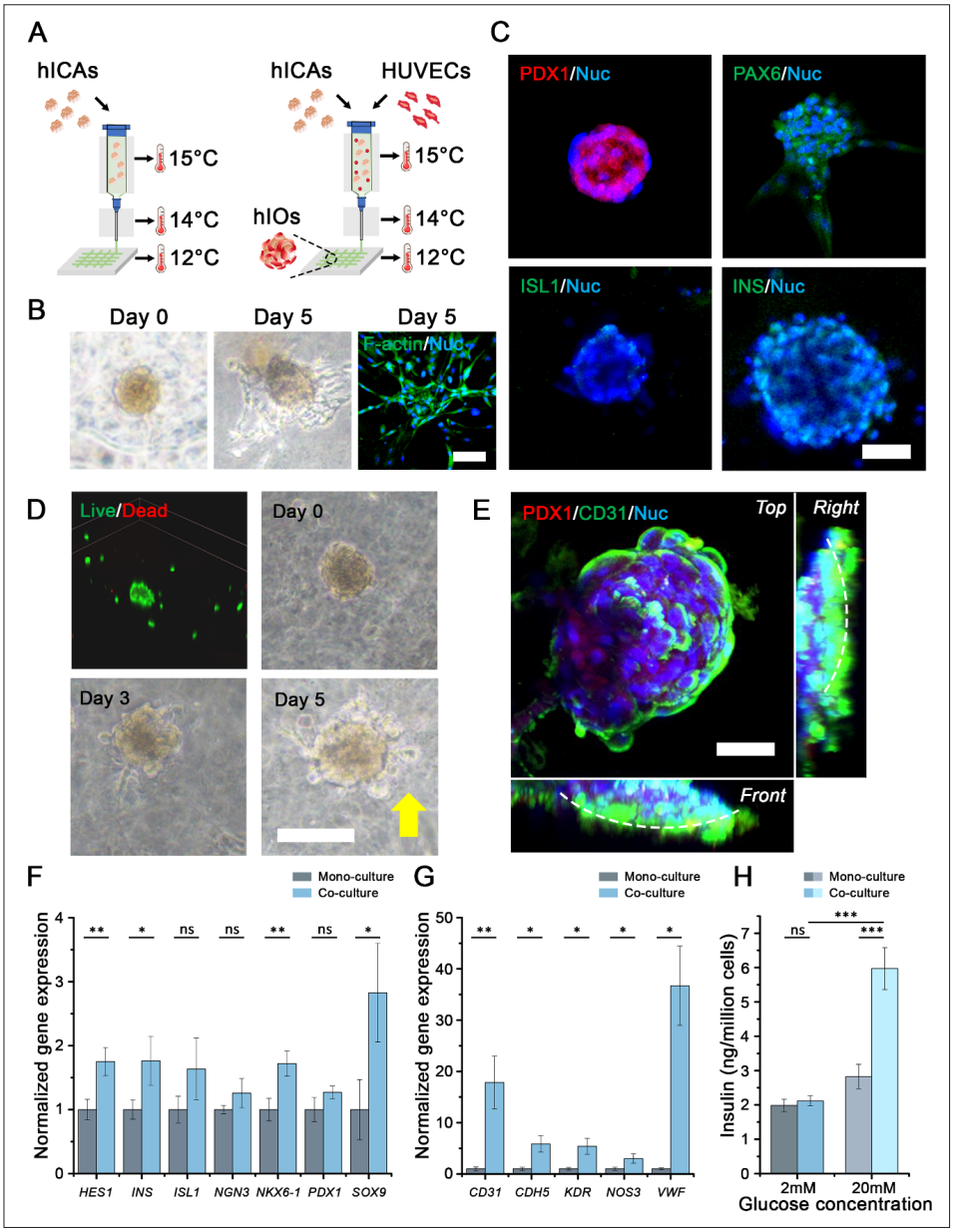

Figure 7. Formation of functional hIOs using 3D bioprinting-based co-culture and cell self-assembly of hICAs and HUVECs. (A) Schematic illustration of 3D bioprinting with hICAs only (left) and 3D bioprinting of hICAs and HUVECs, showing the formation of hIOs (right) under tri-module thermal control. Mono-culture of hICAs: (B) Phase-contrast microscopy images and F-actin staining of printed hICAs during 5 days of culture (scale bar: 50 μm; magnification: 200×). (C) Immunofluorescence images of hICAs in the 3D-bioprinted structure on day 5 showing islet-related proteins (PDX1, PAX6, ISL1, and INS) (scale bar: 50 μm; magnification: 200×). Co-culture of hICAs and HUVECs: (D) Live/dead staining and phase-contrast microscopy images of hICAs (aggregates) and HUVECs (single cells) during culture. The yellow arrow indicates endothelial cells that migrated from the hydrogel and aggregated around hICAs (scale bar: 100 μm; magnification: 200×). (E) 3D projection views of immunofluorescence staining showing the islet marker (PDX1) and HUVEC marker (CD31) on day 5. White dashed curves in the front and right views indicate the aggregate boundary (scale bar: 50 μm; magnification: 200×). (F) Relative gene expression of islet-related markers (*HES1*, *INS*, *ISL1*, *NGN3*, *NKX6-1*, *PDX1*, and *SOX9*) in mono-culture (hICAs only) and co-culture (hICAs and HUVECs). (G) Relative gene expression of endothelial markers (*CD31*, *CDH5*, *KDR*, *NOS3*, and *VWF*) in mono-culture and co-culture. Gene expression levels were normalized to mono-culture and presented as $2^{-\Delta\Delta Ct}$ ($n = 3$). Statistical analysis was performed using the two-sided Student's *t*-test. Single asterisk (*), double asterisk (**), and triple asterisk (***) indicate statistical significance at $p < 0.05$, $p < 0.01$, and $p < 0.001$, respectively. "ns" denotes no statistical significance. Abbreviations: 3D, three-dimensional; CD31, platelet and endothelial cell adhesion molecule 1 gene (*PECAM1*); CDH5, cadherin 5; F-actin, filamentous actin; *HES1*, Hes family BHLH transcription factor 1 gene; hICA, human islet β-like cell aggregate; hIO, human islet organoid; HUVEC, human umbilical vein endothelial cell; INS, insulin; ISL1, islet 1; KDR, kinase insert domain receptor; NGN3, neurogenin-3; NKX6-1, NK6 homeobox 1; NOS3, nitric oxide synthase 3; PAX6, paired box gene 6; PDX1, pancreatic and duodenal homeobox 1; SOX9, SRY-box transcription factor 9; VWF, von Willebrand factor.

in our hIOs resembled an intermediate stage of development between immature and mature islets, when dispersed single cells had aggregated, spread, and enveloped the islet cells, but were still in the early phase of vascular connection and network formation.[39–41] These findings indicate that vascularized islet tissue containing elongated endothelial structures was successfully developed.

We further evaluated the gene expression of islet-related markers and endothelial markers in the hIOs, compared with that of hICAs without HUVECs. The gene expression of mature, INS-producing β-cell markers (*NKX6-1* and *INS*) was upregulated by 1.7-fold and 1.8-fold, respectively, with statistical significance in hIOs. The gene expression of endocrine progenitor markers (*HES1* and *SOX9*) was upregulated by 1.8-fold and 2.8-fold, respectively, and reached statistical significance. Other islet-related markers, including *ISL1*, *NGN3*, and *PDX1*, showed increasing trends in co-cultured hIOs compared with mono-cultured hICAs, although the differences were not significant (Figure 7F). The hIOs demonstrated increased functional maturity, which is beneficial for rapid INS secretion after transplantation. The enhanced expression of endocrine progenitor markers demonstrated the developmental fidelity of the hIOs, supporting their potential to continuously generate islet-like cells after transplantation. The gene expression of endothelial markers, including *CD31*, *CDH5*, *KDR*, *NOS3*, and *VWF*, was upregulated by 17.8-fold, 5.9-fold, 5.4-fold, 3.0-fold, and 36.7-fold, respectively, in hIOs, all with statistical significance, thereby validating the role of HUVECs in promoting islet maturation as supporting cells (Figure 7G). This finding is consistent with a previous report showing that endothelial cells specifically enhance the *INS* gene expression in islet endocrine cells.[38]

Finally, we performed the GSIS assay to evaluate the glucose-responsive insulin secretory function of hIOs (Figure 7H). hIOs showed a significant increase in INS secretion, rising from 2.12 to 5.97 ng/million cells, with a GSIS index of 2.8, whereas mono-cultured hICAs did not show a significant response. The comparison between hIOs and hICAs highlights the importance of endothelial cells in enhancing INS secretion. Although our hIOs exhibited lower levels of INS secretion compared with most ESC- or iPSC-derived β-cells, the GSIS index was comparable.[42–44] This may be attributed to the differentiation strategy and cell purity, as those studies employed more complex differentiation processes from pluripotent stem cells, where only mature β-cells were sorted for use. Our hIOs more closely resembled a complex islet structure *in vivo*, while the INS-producing cells within the hIOs exhibited a similar glucose response to those in other studies, highlighting the importance of endothelial cells in islet functional maturation.

These results indicate that the combination of a printed mesh structure with supporting endothelial cells, appropriate scaffold stiffness, and porous bioactive bioinks established a biomimetic environment that facilitates the formation of hIOs *in vitro*. Using PUMP and bioprint-based co-culture, we can produce these hIOs at a large scale with reduced costs for both research and clinical applications, which represents a significant improvement over traditional methods. The use of hADSCs and HUVECs also potentially reduces immune responses in future transplantation. These hIOs, with a defined structure incorporating vascular elements and glucose-responsive function, hold potential for studies of vascularization, pancreatic development, drug screening, and islet transplantation.

4. Conclusion

In this study, we demonstrated the successful large-scale production of functional vascularized hIOs through a 3D bioprinting-based co-culture and cell self-assembly approach. By employing the PUMP system with optimized stiffness, we generated uniform hICAs from hADSCs. The integration of a tri-module bioprinting process with a ternary gelatin–alginate–Matrigel bioink enabled the bioprinting of hICAs and HUVECs to form hIOs through co-culture and self-assembly. These organoids were structurally and functionally similar to human islets, exhibiting upregulated expression of endocrine progenitor and mature β-cell markers, and demonstrated GSIS. This approach provides a scalable and biologically relevant novel hIO model, advancing applications in vascularization studies, pancreatic development research, drug screening, and islet transplantation for diabetes therapy.

Acknowledgments

None.

Funding

This study was supported by the National Key Research and Development Program of China (2022YFA1104600; 2018YFA0109000).

Conflict of interest

The authors declare that they have no conflict of interest.

Author contributions

Conceptualization: Rui Yao, Yijun Su, Supeng Ding
Formal analysis: Yijun Su, Supeng Ding

Funding acquisition: Rui Yao, Mingen Xu
Investigation: Supeng Ding, Yijun Su, Yinying Lu, Yongyong Zhou
Methodology: Supeng Ding, Yijun Su, Yongyong Zhou
Project administration: Rui Yao, Mingen Xu, Feng Lin
Visualization: Yijun Su, Supeng Ding
Writing–original draft: Yijun Su, Supeng Ding
Writing–review & editing: Rui Yao, Supeng Ding, Yijun Su, Tiankun Liu

Ethics approval and consent to participate

Not applicable.

Consent for publication

Not applicable.

Availability of data

Data is available from the corresponding author upon reasonable request.

References

1. Sun H, Saeedi P, Karuranga S, *et al*. IDF Diabetes Atlas: global, regional and country-level diabetes prevalence estimates for 2021 and projections for 2045. *Diabetes Res Clin Pract*. 2022;183:109119. doi: 10.1016/j.diabres.2021.109119
2. Chhabra P, Brayman KL. Overcoming barriers in clinical islet transplantation: current limitations and future prospects. *Curr Probl Surg*. 2014;51(2):49-86. doi: 10.1067/j.cpsurg.2013.10.002
3. Kim Y, Kim H, Ko UH, *et al*. Islet-like organoids derived from human pluripotent stem cells efficiently function in the glucose responsiveness in vitro and in vivo. *Sci Rep*. 2016;6:35145. doi: 10.1038/srep35145
4. Liang S, Su Y, Yao R. 3D bioprinting of induced pluripotent stem cells and disease modeling. In: Kuehn MH, Zhu W, eds. *Human iPSC-derived Disease Models for Drug Discovery*. Handbook of experimental pharmacology. Springer, Cham. 2023; vol 281: 29-56. doi: 10.1007/164_2023_646
5. Candiello J, Grandhi TSP, Goh SK, *et al*. 3D heterogeneous islet organoid generation from human embryonic stem cells using a novel engineered hydrogel platform. *Biomaterials*. 2018;177:27-39. doi: 10.1016/j.biomaterials.2018.05.031
6. Liang S, Luo Y, Su Y, *et al*. Distinct toxicity of microplastics/TBBPA co-exposure to bioprinted liver organoids derived from hiPSCs of healthy and patient donors. *Int J Bioprint*. 2024;10(3):1403. doi: 10.36922/ijb.1403
7. de Klerk E, Hebrok M. Stem cell-based clinical trials for diabetes mellitus. *Front Endocrinol (Lausanne)*. 2021;12:631463. doi: 10.3389/fendo.2021.631463
8. Panes J, Garcia-Olmo D, Van Assche G, *et al*. Long-term efficacy and safety of stem cell therapy (Cx601) for complex perianal fistulas in patients with Crohn's disease. *Gastroenterology*. 2018;154(5):1334-1342.e4. doi: 10.1053/j.gastro.2017.12.020
9. Hong Y, Park EY, Kim D, Lee H, Jung HS, Jun HS. Glucosamine potentiates the differentiation of adipose-derived stem cells into glucose-responsive insulin-producing cells. *Ann Transl Med*. 2020;8(8):561. doi: 10.21037/atm.2020.03.103
10. Dave SD, Vanikar AV, Trivedi HL. Extrinsic factors promoting in vitro differentiation of insulin-secreting cells from human adipose tissue-derived mesenchymal stem cells. *Appl Biochem Biotechnol*. 2013;170(4):962-71. doi: 10.1007/s12010-013-0250-y
11. Wang X, Luo Y, Ma Y, Wang P, Yao R. Converging bioprinting and organoids to better recapitulate the tumor microenvironment. *Trends Biotechnol*. 2024;42(5):648-663. doi: 10.1016/j.tibtech.2023.11.006
12. Luo Y, Luo L, Wang L, *et al*. Large-scale bioprinting of human epiblast-like models featuring disc-shaped morphogenesis and gastrulation events. *Adv Sci (Weinh)*. 2025;12(33):e05340. doi: 10.1002/advs.202505340
13. Marchioli G, van Gurp L, van Krieken PP, *et al*. Fabrication of three-dimensional bioplotted hydrogel scaffolds for islets of Langerhans transplantation. *Biofabrication*. 2015;7(2):025009. doi: 10.1088/1758-5090/7/2/025009
14. Song J, Millman JR. Economic 3D-printing approach for transplantation of human stem cell-derived beta-like cells. *Biofabrication*. 2016;9(1):015002. doi: 10.1088/1758-5090/9/1/015002
15. Hwang DG, Jo Y, Kim M, *et al*. A 3D bioprinted hybrid encapsulation system for delivery of human pluripotent stem cell-derived pancreatic islet-like aggregates. *Biofabrication*. 2021;14(1). doi: 10.1088/1758-5090/ac23ac
16. Kim J, Shim IK, Hwang DG, *et al*. 3D cell printing of islet-laden pancreatic tissue-derived extracellular matrix bioink constructs for enhancing pancreatic functions. *J Mater Chem B*. 2019;7(10):1773-1781. doi: 10.1039/c8tb02787k
17. Idaszek J, Volpi M, Paradiso A, *et al*. Alginate-based tissue-specific bioinks for multi-material 3D-bioprinting of pancreatic islets and blood vessels: a step towards vascularized pancreas grafts. *Bioprinting*. 2021;24:e00163. doi: 10.1016/j.bprint.2021.e00163

18. Yao R, Wang J, Li X, *et al*. Hepatic differentiation of human embryonic stem cells as microscaled multilayered colonies leading to enhanced homogeneity and maturation. *Small*. 2014;10(21):4311-4323.
doi: 10.1002/smll.201401040

19. Costa EC, de Melo-Diogo D, Moreira AF, Carvalho MP, Correia IJ. Spheroids formation on non-adhesive surfaces by liquid overlay technique: considerations and practical approaches. *Biotechnol J*. 2018;13(1).
doi: 10.1002/biot.201700417

20. Ansari A, Trehan R, Watson C, Senyo S. Increasing silicone mold longevity: a review of surface modification techniques for PDMS-PDMS double casting. *Soft Mater*. 2021; 19(4):388-399.
doi: 10.1080/1539445x.2020.1850476

21. Clark CT, Wang Y, Johnson DC, Lee SC, Smith Q. Effects of PDMS culture on stem cell differentiation towards definitive endoderm and hepatocytes. *Acta Biomater*. 2025; 200:508-519.
doi: 10.1016/j.actbio.2025.05.017

22. Anitha R, Vaikkath D, Shenoy SJ, Nair PD. Tissue-engineered islet-like cell clusters generated from adipose tissue-derived stem cells on three-dimensional electrospun scaffolds can reverse diabetes in an experimental rat model and the role of porosity of scaffolds on cluster differentiation. *J Biomed Mater Res A*. 2020;108(3):749-759.
doi: 10.1002/jbm.a.36854

23. Nyitray CE, Chavez MG, Desai TA. Compliant 3D microenvironment improves β-cell cluster insulin expression through mechanosensing and β-catenin signaling. *Tissue Eng Part A*. 2014;20(13-14):1888-1895.
doi: 10.1089/ten.tea.2013.0692

24. Tran R, Moraes C, Hoesli CA. Developmentally-inspired biomimetic culture models to produce functional islet-like cells from pluripotent precursors. *Front Bioeng Biotechnol*. 2020;8:583970.
doi: 10.3389/fbioe.2020.583970

25. Ding S, Feng L, Wu J, Zhu F, Tan Z, Yao R. Bioprinting of stem cells: interplay of bioprinting process, bioinks, and stem cell properties. *ACS Biomater Sci Eng*. 2018; 4(9):3108-3124.
doi: 10.1021/acsbiomaterials.8b00399

26. Chen R, Su Y, Chen D, *et al*. Bioprinting with superelastic and fatigue-resistant bioinks for large-sized tissue delivery. *Int J Bioprint*. 2024;10(5):3898.
doi: 10.36922/ijb.3898

27. Cahn F. Biomaterials aspects of porous microcarriers for animal cell culture. *Trends Biotechnol*. 1990;8(5):131-136.
doi: 10.1016/0167-7799(90)90154-P

28. Ouyang L, Yao R, Mao S, Chen X, Na J, Sun W. Three-dimensional bioprinting of embryonic stem cells directs highly uniform embryoid body formation. *Biofabrication*. 2015;7(4):044101.
doi: 10.1088/1758-5090/7/4/044101

29. Yao R, Zhang R, Luan J, Lin F. Alginate and alginate/gelatin microspheres for human adipose-derived stem cell encapsulation and differentiation. *Biofabrication*. 2012;4(2):025007.
doi: 10.1088/1758-5082/4/2/025007

30. Townsend SE, Gannon M. Extracellular matrix-associated factors play critical roles in regulating pancreatic beta-cell proliferation and survival. *Endocrinology*. 2019; 160(8):1885-1894.
doi: 10.1210/en.2019-00206

31. Parvaneh S, Kemeny L, Ghaffarinia A, Yarani R, Vereb Z. Three-dimensional bioprinting of functional beta-islet-like constructs. *Int J Bioprint*. 2023;9(2):665.
doi: 10.18063/ijb.v9i2.665

32. Wex C, Frohlich M, Brandstadter K, Bruns C, Stoll A. Experimental analysis of the mechanical behavior of the viscoelastic porcine pancreas and preliminary case study on the human pancreas. *J Mech Behav Biomed Mater*. 2015;41:199-207.
doi: 10.1016/j.jmbbm.2014.10.013

33. Aplin AC, Aghazadeh Y, Mohn OG, Hull-Meichle RL. Role of the pancreatic islet microvasculature in health and disease. *J Histochem Cytochem*. 2024;72(11-12):711-728.
doi: 10.1369/00221554241299862

34. Lammert E, Cleaver O, Melton D. Induction of pancreatic differentiation by signals from blood vessels. *Science*. 2001;294(5542):564-567.
doi: 10.1126/science.1064344 .

35. Wang X, Ye K. Three-dimensional differentiation of embryonic stem cells into islet-like insulin-producing clusters. *Tissue Eng Part A*. 2009;15(8):1941-1952.
doi: 10.1089/ten.tea.2008.0181

36. Aghazadeh Y, Poon F, Sarangi F, *et al*. Microvessels support engraftment and functionality of human islets and hESC-derived pancreatic progenitors in diabetes models. *Cell Stem Cell*. 2021;28(11):1936-1949.e8.
doi: 10.1016/j.stem.2021.08.001

37. Jaramillo M, Mathew S, Mamiya H, Goh SK, Banerjee I. Endothelial cells mediate islet-specific maturation of human embryonic stem cell-derived pancreatic progenitor cells. *Tissue Eng Part A*. 2015;21(1-2):14-25.
doi: 10.1089/ten.tea.2014.0013

38. Zanone MM, Favaro E, Camussi G. From endothelial to beta cells: insights into pancreatic islet microendothelium. *Curr Diabetes Rev*. 2008;4(1):1-9.
doi: 10.2174/157339908783502415

39. Glorieux L, Sapala A, Willnow D, *et al*. Development of a 3D atlas of the embryonic pancreas for topological and quantitative analysis of heterologous cell interactions. *Development*. 2022;149(3):dev199655.
doi: 10.1242/dev.199655

40. Ranjan AK, Joglekar MV, Hardikar AA. Endothelial cells in pancreatic islet development and function. *Islets*. 2009;1(1):2-9.
doi: 10.4161/isl.1.1.9054

41. Mateus Goncalves L, Almaca J. Functional characterization of the human islet microvasculature using living pancreas slices. *Front Endocrinol (Lausanne)*. 2020;11:602519.
doi: 10.3389/fendo.2020.602519

42. Velazco-Cruz L, Song J, Maxwell KG, *et al*. Acquisition of dynamic function in human stem cell-derived beta cells. *Stem Cell Rep*. 2019;12(2):351-365.
doi: 10.1016/j.stemcr.2018.12.012

43. Velazco-Cruz L, Goedegebuure MM, Maxwell KG, Augsornworawat P, Hogrebe NJ, Millman JR. SIX2 regulates human beta cell differentiation from stem cells and functional maturation in vitro. *Cell Rep*. 2020; 31(8):107687.
doi: 10.1016/j.celrep.2020.107687

44. Cardenas-Diaz FL, Osorio-Quintero C, Diaz-Miranda MA, *et al*. Modeling monogenic diabetes using human ESCs reveals developmental and metabolic deficiencies caused by mutations in HNF1A. *Cell Stem Cell*. 2019;25(2):273-289.e5.
doi: 10.1016/j.stem.2019.07.007